PHYSICAL REVIEW B VOLUME 10, NUMBER 12 15 DECEMBER 1974

Investigation of the low-temperature thermoelectric properties of tungsten by a field-nulling technique*

J. C. Garland and D. J. VanHarlingen†
Department of Physics, The Ohio State University, Columbus, Ohio 43210
(Received 20 February 1974)

The thermoelectric dc transport properties of five single-crystal tungsten samples have been measured over the temperature range 1.2–7 K. In addition to the electrical resistivity, thermal resistivity, and thermoelectric power, a new thermoelectric function $G(T)$ was determined; the properties of this function and the method for measuring it are analyzed. Evidence for electron-phonon scattering was observed for both the electrical and thermal resistivity, appearing as a deviation from a quadratic temperature dependence usually associated with the electron-electron interaction. The thermoelectric coefficients $S(T)$ and $G(T)$ were positive below about 5 K for all samples with a sign reversal occurring at higher temperatures. Below 3 K, a marked impurity dependence in the thermoelectric properties was observed. No sample exhibited the characteristic temperature dependence of electron-electron scattering. The sign reversal at higher temperatures is attributed to the onset of a phonon-drag mechanism.

I. INTRODUCTION

The electronic properties of tungsten have been the subject of considerable interest in recent years. Having a $5d^4$, $6s^2$ atomic configuration, tungsten resembles in many ways its $4d^5$, $5s^1$ neighbor in the second transition series, molybdenum. Each element is nonmagnetic, completely compensated, and has a closed Fermi surface consisting of several relatively simple topological shapes. Tungsten, in particular, has been the object of extensive theoretical and experimental Fermi-surface studies, so that the details of its electronic structure are now reasonably well understood.[1] The metal is characterized by a significant hybridization of s- and d-like electron states, so that the model of a high-density d band and a mobile, low-density s band[2] which is frequently advanced for transition metals has little validity.

While the electronic structure of tungsten has been studied thoroughly, relatively little is known about scattering processes in the metal[3] despite the fact that samples of tungsten can be readily prepared (by zone refining) into ultrapure single-crystal form. It is widely believed that electron-electron scattering between Fermi-surface sheets should dominate the low-temperature scattering in the nonmagnetic transition metals,[4] and in fact, most of the electrical resistivity measurements reported for these elements[3] show the quadratic temperature dependence characteristic of the electron-electron interaction. In tungsten, however, electron-electron scattering is not expected to be as significant a process as in the other transition metals. The low-temperature electronic specific heat of tungsten is only about 1 mJ/K^2 mole,[5] well below that of any other metal in the transition-metal series, and it may be inferred from this that the electronic density of states—and hence the predominance of electron-electron scattering—is quite low. Nevertheless, measurements by Wagner *et al.*[6] of the electrical resistance and the analogous thermal quantity WT (W is the thermal resistivity) of tungsten have shown that each varies nearly as T^2 over the temperature range 1–5 K. While these results were explained at the time on the basis of electron-electron scattering, a more recent study, by Wagner,[7] of the high-field electrical and thermal magnetoconductivity of tungsten obtained results that could not be explained plausibly by electron-electron scattering; instead it was suggested that the electron-phonon interaction might be responsible not only for the observed galvanomagnetic effects, but also for the earlier low-temperature zero-field measurements. It was primarily these results that provided the stimulus for the investigation of the low-temperature thermoelectric properties of tungsten which is reported here.[8]

Previous measurements of the thermoelectric properties of tungsten are very sparse. Raag and Kowger[9] investigated the temperature dependence of the thermoelectric power of tungsten above 400 K and found it to be positive, varying between 5 and 20 μV/K. These results were consistent with earlier measurements by Lander[10] of the high-temperature Thomson coefficient. The thermoelectric power of two polycrystalline tungsten wires was measured by Carter, Davidson, and Schroeder,[11] over the temperature range 5–300 K. They found the thermoelectric power of each specimen to be negative between approximately 15 and 270 K and positive below 15 K. A peak was observed in S near 10 K of about 0.1 μV/K which was most pronounced in the lower-purity specimen. This low-

temperature peak was attributed to phonon-drag effects resulting from electronic transitions across the small hole ellipsoids centered at the symmetry point N. (At low temperatures, transitions across the larger surfaces would not be significant because of insufficient phonon energy.) It is interesting to note that these hole ellipsoids comprise only about 11% of the available Fermi-surface area of tungsten[12] and thus can be considered to play only a minor role in electrical conduction. An alternate explanation of the peak was made by Colquitt, Fankhauser, and Blatt,[13] who suggested that it might result from a positive diffusion term in the thermoelectric power arising from electron-electron scattering in combination with a higher-temperature negative term due to electron-phonon scattering. A very recent study of the thermoelectric power of a pure single crystal of tungsten from 2 to 9 K by Trodahl[14] confirmed the existence of the positive low-temperature peak in S; Trodahl interpreted his results on the basis of a positive electron-electron diffusion term at low temperatures which becomes swamped at higher temperatures by a negative phonon-drag peak. He also found, however, that a combination of an impurity term and a low-temperature phonon-drag term provided an equally satisfactory fit to his data below 4 K. To summarize the results of the measurements we have made of the thermoelectric properties of tungsten, we find no evidence for electron-electron scattering at low temperatures, but we do believe that the low-temperature positive peak in the thermopower is a result of the "tail" of a large negative phonon-drag peak whose maximum occurs about 70 K.

In our measurements of the thermoelectric properties of five tungsten samples, we have made use of a new technique which we believe can offer substantial benefits over conventional thermoelectric-power experiments under certain circumstances. There are basically two problems to be overcome in determining the thermoelectric power of a very pure metal at low temperatures: The thermoelectric voltages are very small, typically 10^{-11} V, and temperature differences of only a few millidegrees must be accurately measured. While the discovery of the dc Josephson effect now makes it possible to measure very small voltages with great accuracy,[15] there nevertheless remains the difficult thermometry problem of determining tiny temperature gradients with microdegree resolution. In the technique we have used, temperature differences are not measured; instead, our method involves the measurement of two currents, a heat current and an electric current, while a voltmeter is used only as a null detector. We do not obtain the thermoelectric power from this method [although in the work reported here we also measured $S(T)$ of our samples using conventional techniques] but instead a related thermoelectric function $G(T)$. The properties of this function are discussed in Sec. II, but we mention here that $G(T)$ exhibits the same, or greater, sensitivity to scattering processes as the thermopower, and in pure metals can be measured with at least an order-of-magnitude improvement in resolution over comparable measurements of $S(T)$.

II. THERMOELECTRIC FUNCTION $G(T)$

A. Basic concepts

In metals, the flow of heat current and electric current can be specified quite generally by two linear transport equations of the form[16]

$$\vec{J} = e^2 K_0 \vec{E} + (e/T) K_1 (-\vec{\nabla} T) , \tag{1}$$

$$\vec{J}_Q = e K_1 \vec{E} + (1/T) K_2 (-\vec{\nabla} T) , \tag{2}$$

where the electric current $\vec{J}$ and the heat current $\vec{J}_Q$ are coupled together by a common thermoelectric transport coefficient K_1.[17] Because K_1 is not a directly accessible experimental quantity, measurements of it are usually made in combination with other coefficients, for example, the thermoelectric power $S = (1/eT) K_1 K_0^{-1}$, or the Peltier coefficient $\pi = (1/e) K_1 K_0^{-1}$.

In this section we wish to introduce another thermoelectric parameter G, which we believe can provide useful information about the thermoelectric properties of metals, particularly under circumstances which make conventional thermopower measurements very difficult. G is defined by

$$G = e K_1 K_2^{-1} \tag{3}$$

and is functionally similar to the thermoelectric power S, except for the substitution of the thermal conductivity K_2/T (appropriate to $\vec{E} = 0$ rather than $\vec{J} = 0$) for the electrical conductivity $e^2 K_0$. This relationship can be expressed formally in terms of the Wiedemann-Franz ratio by noting that

$$\begin{aligned} S/G &= (1/eT) K_1 K_0^{-1} / (e K_1 K_2^{-1}) \\ &= (K_2/T)/(e^2 K_0) = LT , \end{aligned} \tag{4}$$

where the Wiedemann-Franz ratio L reduces to the classical Lorenz number L_0 under conditions of elastic scattering. Equation (4) suggests that $S/L_0 T$ is the appropriate quantity for comparing measurements of G and S, their ratio providing an indication of the extent of inelastic scattering events, i.e.,

$$(S/L_0 T)/G = L/L_0 . \tag{5}$$

Strictly speaking, Eqs. (4) and (5) are in error by a term of order $(k_B T/\mu)^2$ which arises from the difference between K_2/T and the usual definition of the thermal conductivity $\kappa = (1/T)(K_2 - K_1^2 K_0^{-1})$ (de-

termined in the absence of an electric current flow). Although this term is of no experimental consequence in metals at low temperatures, it does have thermodynamic implications for this work, as will be shown subsequently.

It is possible to make direct measurements of G by applying a heat current $\vec{J}_Q$ to a specimen and then balancing out the resulting thermoelectric voltage gradient with an opposing electric current $\vec{J}$. From Eqs. (1) and (2), it follows that for $\vec{E}=0$,

$$G = J/J_Q \ , \tag{6}$$

where $\vec{E}$ is the "effective" electric field given by $\vec{E} = -(1/e)\vec{\nabla}(\mu + eV)$.

Although the details of this field-nulling technique will be discussed in Sec. III, we mention here that in pure metals at low temperatures it is possible to measure these two currents with better precision than the fields $\vec{E}$ and $\vec{\nabla}T$ which are required for thermoelectric-power calculations.

B. Thermodynamic considerations

The currents $\vec{J}$ and $\vec{J}_Q$ which are used to determine the thermoelectric function G are measured under conditions of a uniform electrochemical potential ϕ, given by

$$e\phi = \mu + eV \ . \tag{7}$$

In this situation the usual field-derived energy source $\vec{J}\cdot(-\vec{\nabla}\phi)$ is absent, and we wish now to consider the implications of this on the reversible and irreversible processes which normally accompany the simultaneous flow of $\vec{J}$ and $\vec{J}_Q$ in a conductor. We begin by defining an energy current density $\vec{J}_U$ given by

$$\vec{J}_U = \vec{J}_Q + \phi\vec{J} \ . \tag{8}$$

The rate at which energy is supplied to the medium when the electrochemical potential is constant is then

$$-\vec{\nabla}\cdot\vec{J}_U = \vec{\nabla}\cdot\vec{J}_Q + (-\vec{\nabla}\phi)\cdot\vec{J} - \phi\vec{\nabla}\cdot\vec{J} \ , \tag{9}$$

where the last two terms on the right are zero. From Eq. (2) we see that $\vec{J}_Q = (K_2/T)(-\vec{\nabla}T)$ for $\vec{\nabla}\phi = 0$, so that

$$-\vec{\nabla}\cdot\vec{J}_U = -\vec{\nabla}\cdot\left(\frac{K_2}{T}(-\vec{\nabla}T)\right). \tag{10}$$

According to Eq. (10) the only source of energy flow in a measurement of G comes from the ordinary irreversible process of heat conduction from one reservoir to another. The absence of terms corresponding to the Thomson heat and the Joule heat in Eq. (10) does not mean, however, that these effects are nonexistent, but rather that the additional energy for these processes is derived from the heat reservoir instead of the electric field. This may be seen by comparing Eq. (10) with the equivalent expression for the energy flow which occurs when the electric current is absent. We have, for this second case,

$$-\vec{\nabla}\cdot\vec{J}_U = -\vec{\nabla}\cdot[\kappa(-\vec{\nabla}T)] \ , \tag{11}$$

where the thermal conductivity κ is that applicable to the condition that $\vec{J}=0$ rather than $\vec{\nabla}\phi=0$ and is smaller than K_2/T by an amount equal to $K_1^2K_0^{-1}/T$. It may be verified by direct calculation that this difference accounts exactly for the Thomson and Joule effects; it is somewhat more informative, however, to approach this problem from a slightly different point of view.

Consider a conducting medium which supports a fixed temperature gradient $\vec{\nabla}T$ and which has volume densities of energy U and entropy S with associated continuity equations

$$\frac{\partial U}{\partial t} + \vec{\nabla}\cdot\vec{J}_U = 0 \ , \tag{12}$$

$$\frac{\partial S}{\partial t} + \vec{\nabla}\cdot\vec{J}_S = \frac{\partial S_{\rm irr}}{\partial t} \ . \tag{13}$$

Here $\vec{J}_S$ represents an entropy density current equal to $\vec{J}_Q/T$, and we are supposing that the total entropy S is composed of two sources, an "equilibrium" entropy S_0 which can be associated with nondissipative processes, and an "irreversible" entropy $S_{\rm irr}$; $\partial S_{\rm irr}/\partial t$ then corresponds to the rate of entropy production by dissipative processes in a unit volume of the medium. We now wish to calculate the increase in the rate of change of both $S_{\rm irr}$ and S_0 when an electric current $\vec{J}$ is applied to the medium and adjusted so that the electrochemical potential ϕ is uniform. In other words, we want to know

$$\Delta\dot{S}_{\rm irr} = \left(\frac{\partial S_{\rm irr}}{\partial t}\right)_{\vec{\nabla}\phi=0} - \left(\frac{\partial S_{\rm irr}}{\partial t}\right)_{\vec{J}=0} \ , \tag{14}$$

$$\Delta\dot{S}_0 = (-\vec{\nabla}\cdot\vec{J}_S)_{\vec{\nabla}\phi=0} - (-\vec{\nabla}\cdot\vec{J}_S)_{\vec{J}=0} \ . \tag{15}$$

Excluding the possibility of mechanical work on the system, but allowing for the diffusion of charge carriers (as might be encountered in ionic conductors) we have

$$dU = T\,dS + e\phi\,dN \ , \tag{16}$$

where the electrochemical potential ϕ is defined by Eq. (7). Taking the time derivative of Eq. (16) and making use of Eqs. (12) and (13) results in

$$\frac{\partial S}{\partial t} = \frac{1}{T}\frac{\partial U}{\partial t} - \frac{e\phi}{T}\frac{\partial N}{\partial t} \ , \tag{17}$$

$$\frac{\partial S_{\rm irr}}{\partial t} = +\vec{\nabla}\cdot\vec{J}_S - \frac{1}{T}(\vec{\nabla}\cdot\vec{J}_U) + \frac{e\phi}{T}\left(\vec{\nabla}\cdot\frac{\vec{J}}{e}\right) \tag{18}$$

$$= +\vec{\nabla}\cdot\vec{J}_S - \left[\vec{\nabla}\cdot\left(\frac{\vec{J}_U}{T}\right) - \vec{J}_U\cdot\vec{\nabla}\left(\frac{1}{T}\right)\right]$$

$$+\left[\vec{\nabla}\cdot\left(\frac{\phi\vec{J}}{T}\right)-\vec{J}\cdot\vec{\nabla}\left(\frac{\phi}{T}\right)\right]$$

$$=\vec{J}_U\cdot\vec{\nabla}\left(\frac{1}{T}\right)-\vec{J}\cdot\vec{\nabla}\left(\frac{\phi}{T}\right). \tag{19}$$

Using Eq. (19) to solve for $\Delta\dot{S}_{\rm irr}$ we find

$$\Delta\dot{S}_{\rm irr}=(\vec{J}_U-\phi\vec{J})_{\vec{\nabla}\phi=0}\cdot\vec{\nabla}\left(\frac{1}{T}\right)-(\vec{J}_U)_{\vec{J}=0}\cdot\vec{\nabla}\left(\frac{1}{T}\right)$$

$$=\frac{K_2}{T}(-\vec{\nabla}T)\cdot\vec{\nabla}\left(\frac{1}{T}\right)-\left(\frac{K_2-K_1^2K_0^{-1}}{T}\right)(-\vec{\nabla}T)\cdot\vec{\nabla}\left(\frac{1}{T}\right)$$

$$=\frac{K_1^2K_0^{-1}}{T^3}(-\vec{\nabla}T)\cdot(-\vec{\nabla}T). \tag{20}$$

By noting that the electrical conductivity of the medium is $\sigma=e^2K_0$ and that the electric current $\vec{J}=(e/T)K_1(-\vec{\nabla}T)$, where ϕ is uniform, we see that Eq. (20) becomes

$$\Delta\dot{S}_{\rm irr}=\frac{1}{T}\left(\frac{J^2}{\sigma}\right). \tag{21}$$

In other words, the increase in the volume rate of production of entropy in the medium is just that produced by the Joule heat. Experimentally, the source of this entropy production is the increased heat current required to maintain a constant temperature gradient when the electric current is applied; energy is not supplied by the source of electric current since $\vec{\nabla}\phi=0$.

We can now calculate $\Delta\dot{S}_0$ from Eq. (15):

$$\Delta\dot{S}_0=\left(-\vec{\nabla}\cdot\frac{\vec{J}_Q}{T}\right)_{\vec{\nabla}\phi=0}-\left(-\vec{\nabla}\cdot\frac{\vec{J}_Q}{T}\right)_{\vec{J}=0}$$

$$=-\vec{\nabla}\cdot\frac{1}{T}\left[\left(\frac{K_2}{T}-K\right)(-\vec{\nabla}T)\right]$$

$$=\vec{\nabla}\cdot\left(K_1^2K_0^{-1}\frac{\vec{\nabla}T}{T^2}\right). \tag{22}$$

By noting that the thermoelectric power $S=(1/eT)\times K_1K_0^{-1}$ and that $\vec{J}=(e/T)K_1(-\vec{\nabla}T)$, Eq. (22) becomes

$$\Delta\dot{S}_0=-\vec{\nabla}\cdot(S\vec{J})$$

$$=-\frac{1}{T}\left(T\frac{dS}{dT}\vec{\nabla}T\cdot\vec{J}\right)=-\frac{1}{T}(\mu_T\vec{\nabla}T\cdot\vec{J}), \tag{23}$$

where μ_T is the Thomson coefficient and the quantity in brackets on the right is the Thomson heat. Thus the accumulation or depletion of the equilibrium entropy S_0 can be identified with the nondissipative Thomson heat. In measurements of G the Thomson heat is comparable in magnitude to the Joule heat as may be seen from Eq. (1) by noting that $\vec{E}\cdot\vec{J}=0$, and by making use of the Kelvin relation $\mu_T=T(dS/dT)$; i.e.,

$$\vec{J}^2/\sigma+S\vec{\nabla}T\cdot\vec{J}=0. \tag{24}$$

In many simple metals S has a predominantly linear temperature dependence at low temperatures so that $\mu_T\approx S$ and the Joule heat is just absorbed by the Thomson heat.

C. Evaluation of $G(T)$

A general expression for $G(T)$ may easily be derived which is analogous to the familiar formula for the thermoelectric power[18]:

$$S(T)=eL_0T\left(\frac{\partial\ln\sigma(\epsilon)}{\partial\epsilon}\right)_\mu, \tag{25}$$

where $\sigma(\epsilon)$ is the (energy-dependent) conductivity whose derivative is evaluated at the chemical potential. For scattering processes which can be described by a mean free path (assumed to be energy and $\vec{k}$ dependent) the transport coefficients K_0, K_1, and K_2 are given by integrals of the form[19]

$$K_0=\frac{1}{4\pi^3}\int\vec{\lambda}_k^E(\epsilon)\vec{v}_k\left(-\frac{\partial f^0}{\partial\epsilon}\right)d^3k, \tag{26}$$

$$K_1=\frac{1}{4\pi^3}\int\vec{\lambda}_k^T(\epsilon)(\epsilon-\mu)\vec{v}_k\left(-\frac{\partial f^0}{\partial\epsilon}\right)d^3k, \tag{27}$$

$$K_2=\frac{1}{4\pi^3}\int\vec{\lambda}_k^T(\epsilon)(\epsilon-\mu)^2\vec{v}_k\left(-\frac{\partial f^0}{\partial\epsilon}\right)d^3k, \tag{28}$$

where $\vec{\lambda}_k^E(\epsilon)$ and $\vec{\lambda}_k^T(\epsilon)$ are the vector mean free paths resulting from the application of an electric field and a temperature gradient, respectively. If the functional form of the mean free path is the same for each of the coefficients, i.e., if $\vec{\lambda}_k^E(\epsilon)=\vec{\lambda}_k^T(\epsilon)$, then Eq. (26) may be simplified by writing

$$K_0=\int\sigma(\epsilon)\left(-\frac{\partial f^0}{\partial\epsilon}\right)d\epsilon=\sigma(\mu)+\cdots O(k_BT/\mu)^2, \tag{29}$$

where $\sigma(\epsilon)$ is an integral over a constant-energy surface,

$$\sigma(\epsilon)=\frac{e^2}{4\pi^3\hbar}\int\vec{\lambda}_k(\epsilon)\frac{\vec{v}_k}{v_{k_\perp}}dS_k. \tag{30}$$

Using this notation, it ispossible to write the expressions for K_1 and K_2 in terms of $\sigma(\epsilon)$, i.e.,

$$K_1=\frac{1}{e^2}\int(\epsilon-\mu)\sigma(\epsilon)\left(-\frac{\partial f^0}{\partial\epsilon}\right)d\epsilon$$

$$=\frac{1}{e^2}\left[\tfrac{1}{3}(\pi k_BT)^2\left(\frac{\partial\sigma(\epsilon)}{\partial\epsilon}\right)_\mu\right], \tag{31}$$

$$K_2=\frac{1}{e^2}\int(\epsilon-\mu)^2\sigma(\epsilon)\left(-\frac{\partial f^0}{\partial\epsilon}\right)d\epsilon=\frac{1}{e^2}[\tfrac{1}{3}(\pi k_BT)^2\sigma(\mu)]. \tag{32}$$

Dividing Eq. (31) by Eq. (32) we then arrive at the desired result for $G(T)$:

$$G(T)=e\left(\frac{\partial\ln\sigma(\epsilon)}{\partial\epsilon}\right)_\mu. \tag{33}$$

Equation (33) is a general expression in that it allows for an anisotropic and energy-dependent scattering length and also since there are no conditions

or limitations on the Fermi surface of the metal under investigation. On the other hand, the requirement that the mean-free-path function be common to all of the transport coefficients essentially restricts the validity of Eq. (33) to situations in which the scattering is elastic, or at least predominantly elastic.[20] The elastic scattering approximation is likely to be valid in nearly all metals at high temperatures, i.e., for $T \gg \Theta_D$, in alloys, and in pure metals at very low temperatures (when the scattering is dominated by impurities).

Although Eq. (33) bears an interesting resemblence to Eq. (25) for the thermoelectric power, it is in one sense a rather artificial representation for $G(T)$ because of its emphasis on the electrical conductivity. $G(T)$ is a measure of the transport currents in a conductor which result from the application of a temperature gradient. The nonequilibrium distribution function which is responsible for these currents is quite different, both in form and sensitivity to scattering processes, from that which results from an electric field. While the elastic scattering restriction makes it possible to find a direct relationship between the two kinds of distribution functions, in the most general case these functions and the currents they produce cannot be simply related. On the other hand, the currents described by K_1 and K_2 are determined by the same distribution function, so that an expression which relates the two coefficients may be derived which is independent of the details of the scattering. This expression can be obtained by noting that K_1 and K_2 can be written quite generally as

$$K_1 \sim \int (\epsilon - \mu)\Omega(\epsilon)\left(-\frac{\partial f^0}{\partial \epsilon}\right)d\epsilon = \tfrac{1}{3}(\pi k_B T)^2\left(\frac{\partial \Omega(\epsilon)}{\partial \epsilon}\right)_\mu , \tag{34}$$

$$K_2 \sim \int (\epsilon - \mu)^2\Omega(\epsilon)\left(-\frac{\partial f^0}{\partial \epsilon}\right)d\epsilon = \tfrac{1}{3}(\pi k_B T)^2\Omega(\mu) , \tag{35}$$

where the energy-dependent function $\Omega(\epsilon)$ incorporates the effects of scattering, as in Eq. (30), but is not equal to $\sigma(\epsilon)$ unless the scattering is elastic. By the same reasoning that leads to Eq. (33) it then follows immediately that

$$G = eK_1K_2^{-1} = e\left(\frac{\partial \ln \kappa(\epsilon)}{\partial \epsilon}\right)_\mu , \tag{36}$$

where $\kappa(\epsilon) = K_2(\epsilon)/T$. By analogy with $\sigma(\epsilon)$, $\kappa(\epsilon)$ may be thought of as the hypothetical thermal conductivity which could be obtained by changing the chemical potential (as by adding or subtracting electrons) without altering the band structure of the metal. The logarithmic derivative of $\kappa(\epsilon)$ which appears in Eq. (36) is thus to be evaluated at the real chemical potential. We remark that for purely elastic scattering Eq. (33) and Eq. (36) imply that

$$\left(\frac{\partial \ln \kappa(\epsilon)}{\partial \epsilon}\right)_\mu = \left(\frac{\partial \ln \sigma(\epsilon)}{\partial \epsilon}\right)_\mu . \tag{37}$$

This result is consistent with the Wiedemann-Franz law.

As an example of the use of Eq. (36), we will calculate $G(T)$ for a metal with a spherical Fermi surface in the simple relaxation-time approximation. Writing $\vec{\lambda}_k = \vec{v}_k\tau$ we have, from Eq. (28),

$$\kappa = \frac{K_2}{T} = \frac{\tau}{T}\int \vec{v}_k\vec{v}_k(\epsilon - \mu)^2\left(-\frac{\partial f^0}{\partial \epsilon}\right)d^3k$$

$$\sim \int (\epsilon - \mu)^2\,\epsilon^{3/2}\left(-\frac{\partial f^0}{\partial \epsilon}\right)d\epsilon$$

$$\sim \tfrac{1}{3}(\pi k_B T)^2\,\mu^{3/2} , \tag{38}$$

so that $G(T) = e[\partial \ln \kappa(\epsilon)/\partial \epsilon]_\mu$ is given by

$$G = 3e/2\mu . \tag{39}$$

Thus, in this very simple system, $G(T)$ is independent of temperature [to order $(k_B T/\epsilon_F)^2$] and inversely proportional to the chemical potential. The same result is obtained for electron-electron scattering; in this latter case a relaxation time $\tau_{ee} = [(\pi k_B T)^2 + (\epsilon - \mu)^2]^{-1}$ is used but the procedure for calculating $G(T)$ remains the same.

D. Multiple scattering and multiband effects

In a conductor whose transport currents are limited by more than one kind of scattering process, an expression for $G(T)$ may be derived which is analogous to the Nordheim-Gorter[21] rule for the thermoelectric power, although of somewhat greater generality. We consider the conductor to be made up of n elements, each element being characterized by its own thermal resistivity W_i, electrical resistivity ρ_i, thermoelectric power S_i, and thermoelectric function G_i. These four parameters are not independent of each other, but are related according to Eq. (5), i.e., $G_i/S_i = W_i/\rho_i$. As shown by de Vroomen *et al.*,[22] if the scattering rates due to each scattering process are additive, so that Matthiessen's rule is obeyed, then the conductor may be treated as if the individual elements are simply connected in series. For a conductor which carries an electric current $\vec{J}$ and a heat current $\vec{J}_Q$, then the requirement that the electric field vanish may be expressed as

$$\vec{J}\sum_i \rho_i + \sum_i S_i\vec{\nabla}T_i = 0 , \tag{40}$$

where $\vec{\nabla}T_i$ is the temperature gradient across the ith element. Rewriting Eq. (40), we obtain

$$0 = J\sum_i \rho_i - J_Q\sum_i S_iW_i = J\sum_i \rho_i - J_Q\sum_i G_i\rho_i , \tag{41}$$

so that

$$G = \frac{J}{J_Q} = \frac{\sum_i G_i \rho_i}{\sum_i \rho_i} \quad . \tag{42}$$

If there are only two predominant scattering mechanisms, then Eq. (42) takes the useful form,

$$G = \frac{G_1 \rho_1 + G_2 \rho_2}{\rho} = G_1 + \frac{(G_2 - G_1)\rho_2}{\rho} \quad . \tag{43}$$

Although Eq. (43) resembles the Nordheim-Gorter expression for the thermoelectric power there is a significant difference in the conditions for the validity of the two expressions. In particular, Eq. (43) does not assume the validity of the Wiedemann-Franz law so that it may be used at temperatures in which small-angle inelastic scattering precludes the use of the Nordheim-Gorter rule.

For a conductor with more than one conduction band it is often convenient to treat each band as independent of the others and, for the purpose of estimating the transport properties, to assume that all the bands are simply connected in parallel. If we associate with each band an electrical conductivity σ_j, thermal conductivity κ_j, thermoelectric power S_j, and thermoelectric function G_j, then it follows immediately that

$$S = \frac{1}{\sigma} \sum \sigma_j S_j \tag{44}$$

and that

$$G = \frac{1}{\kappa} \sum \kappa_j G_j \quad . \tag{45}$$

Equation (44) is a well-known expression[23] and Eq. (45) follows by setting $\sigma_j S_j = \kappa_j G_j$ as in Eq. (5).

III. EXPERIMENTAL PROCEDURE

A. Measurement of $G(T)$

As shown in Sec. II, $G(T)$ is obtained by measuring the ratio of an electric current $\vec{J}$ to a heat current $\vec{J}_Q$ under conditions of vanishing electric field. To determine this ratio, we have used a simple potentiometric circuit which has proved to be very easy to use and capable of precision of 0.1% or better, even in our largest and most pure specimens. A simplified schematic representation of our experiment is shown in Fig. 1(a). One end of a sample is anchored to a heat reservoir at temperature T_0, while the other end is connected to a heating coil. A section of the sample is short circuited by a superconducting galvanometer which indicates a current flow whenever the heater is turned on. In principle, the magnitude of this current flow is equal to the thermoelectric voltage $S\Delta T$ developed between the galvanometer leads (measured under open-circuit conditions) divided by the resistance R of the sample. In practice, the current through the galvanometer is reduced substantially from this amount by the contact resistance r between the superconducting loop and the sample; our measurements indicate that the contact resistance can be as much as an order of magnitude greater than the sample resistance. The galvanometer "deflection" resulting from a thermoelectrically generated current is amplified and used to supply a feedback current $\vec{J}$ to the sample which restores the galvanometer to equilibrium. The measured quantities in the experiment are then the heat current $\vec{J}_Q$, the feedback current $\vec{J}$, and the temperature T_0.

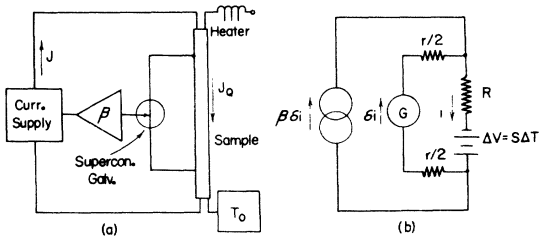

FIG. 1. (a) Simplified diagram of the experiment for measuring the thermoelectric function $G(T)$. (b) Equivalent-circuit representation of the experiment for measuring $G(T)$.

In Fig. 1(b), a simplified equivalent-circuit representation of the experiment is shown in which the sample is treated as a thermoelectric "battery" with internal resistance R and open-circuit voltage $S\Delta T$. The current through the superconducting galvanometer is δi while the feedback current is $\beta\delta i$, β being the effective "open-loop" current gain of the circuit. For the moment we will consider only the equilibrium, steady-state response of the experiment; thus, we will neglect the inductance of the ring formed by the sample and the superconducting galvanometer, as well as the time constants of the feedback circuit. Each of these quantities has an important effect on the stability and response of the experiment and will be considered in detail in the Appendix.

By adding the voltages around the ring consisting of the galvanometer and sample to zero, and by supposing that the current entering or leaving a junction is conserved, we obtain

$$-\Delta V + iR + (\delta i) r = 0 \quad , \tag{46}$$

$$\delta i(\beta + 1) - i = 0 \quad , \tag{47}$$

where i is the current through the sample, r is the total contact resistance between the galvanometer and the sample, $i_0 = \beta(\delta i)$ is the feedback current, and ΔV is the open-circuit thermoelectric voltage developed across the sample. Solving Eqs. (46) and (47) for δi then yields

$$\delta i = \frac{\Delta V}{r + (\beta + 1)R} \approx \frac{\Delta V}{\beta R} \quad \text{for } \beta \gg 1 \quad . \tag{48}$$

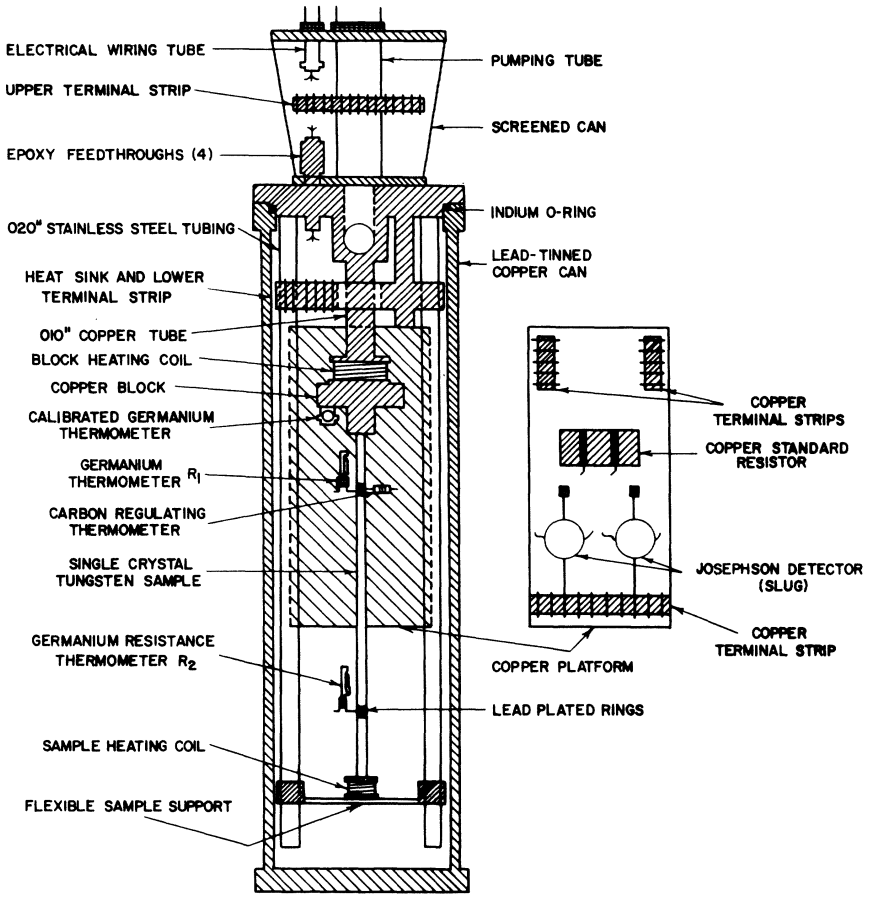

FIG. 2. Diagram of the cryostat used in the experiment.

For a finite current gain β, the equilibrium offset current δi leads to an error in the measurement of G. In order for this feedback error to be smaller than the error introduced by random system noise we require, from Eq. (48), that

$$\beta > \frac{\Delta V}{\epsilon R} , \tag{49}$$

where the over-all system noise is now considered equivalent to an rms noise current in the galvanometer. For characteristic values of $R = 10^{-8}\ \Omega$, $V = 10^{-11}$ V, and $\epsilon = 10^{-7}$ A, we require that the over-all current gain of the system be greater than 10^4 in order for the feedback error to be negligible. The corresponding fractional error in the measurement of G is then easily estimated. From Eq. (48), the feedback current $i_0 = \beta \delta i$ can be written as

$$i_0 = \left(\frac{\beta}{\beta+1}\right) \frac{\Delta V/R}{1 + r/(\beta+1)R} \approx \frac{\Delta V}{R} \left(1 - \frac{r}{\beta R}\right) . \tag{50}$$

The fractional error in G is then given by

$$\frac{\delta G}{G} = \frac{\Delta V/R - i_0}{\Delta V/R}$$

$$\approx \frac{r}{\beta R} . \tag{51}$$

In this experiment, $r \approx 10^{-7}\ \Omega$ and $R \approx 10^{-8}\ \Omega$ so that $\delta G/G \simeq 0.1\%$, a value which corresponded closely to the measured scatter of the data for most of the samples.

B. Experiment details

The cryostat with its associated instrumentation (Figs. 2 and 3) was designed so that measurements of the electrical resistivity ρ, thermal resistivity W, and thermoelectric power S could be taken at each temperature in addition to the thermoelectric function G. The tungsten samples were in the form of cylindrical rods with lengths between 6 and 15 cm and diameters of 1.5 to 7.0 mm. The rods were suspended inside of an evacuated copper can whose inside surface was tinned with lead. A 100-Ω heating coil was attached to one end of the sample. On the larger-diameter samples the coil was wound directly onto the end of the rod and cemented into place with GE 7031 varnish; on the smaller samples the coil was wound onto a hollow copper former and then soldered to a lead band which was

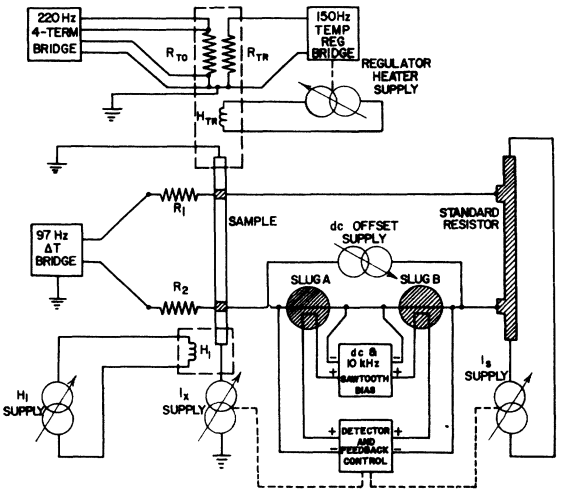

FIG. 3. Diagram of the instrumentation used in the experiment.

electroplated onto the end of the sample. The other end of the sample was attached to a cylindrical copper block which was thermally isolated, via a 0.010-in.-wall copper tube, from the helium bath. The temperature of this block was monitored by a calibrated germanium thermometer in conjunction with a four-terminal ac resistance bridge[24] operating at 220 Hz. An electronic regulator, operating at 150 Hz, was used to maintain the temperature of the sample at a constant value; the regulator heater was wound directly onto the block while the regulator sensing thermometer (an 82-Ω-$\frac{1}{8}$-W composition resistor) was attached to either the sample or to the block itself. The latter arrangement was used when the thermal time constants of the sample and block made it difficult to obtain a stable temperature.

Temperature differences along the sample were measured with matched germanium thermometers R_1 and R_2. These thermometers consisted of bare germanium chips, supplied by Cryocal, Inc., which were mounted onto tiny epoxy holders and soldered to lead bands on the sample. A differential three-wire temperature bridge, operating at 97 Hz, was used to measure R_1 and $\Delta R = R_1 - R_2$. During each run, R_1 and ΔR were calibrated against the germanium standard thermometer at 0.1-K intervals. These calibration points were used as the basis for a least-squares fit to the expression

$$\ln T = a_0 + a_1 \ln R + a_2 \ln^2 R \ . \qquad (52)$$

Once the least-squares coefficients a_0, a_1, and a_2 were determined from the data, the temperature derivatives of R were calculated from the expression [obtained by inverting Eq. (52)]

$$\frac{dR}{dT} = -\frac{R}{T}[a_1^2 - 4a_2(a_0 - \ln T)]^{-1/2} , \qquad (53)$$

where

$$\ln R = -\frac{a_1}{2a_2} - \frac{1}{2a_2}[a_1^2 - 4a_2(a_0 - \ln T)]^{1/2} . \qquad (54)$$

Equation (53) was used to determine the temperature differences along the sample according to a procedure described in a previous paper.[6] Typical values of ΔT varied between 0.1 and 10 mK, corresponding to a heater power of 1–10 mW.

Current and voltage measurements were made using a Josephson junction detector (Clarke "SLUG") as a superconducting galvanometer.[25] Two detectors were used to cover the 1–7-K temperature range, each selected to have desirable switching characteristics at its working temperature. The detectors were ac biased at their critical currents at a frequency of 10 kHz. The technique used for measurements of $G(T)$ has been previously described; voltage measurements used for determining the thermoelectric power and electrical resistance were made by balancing the voltage across the sample with a voltage across a standard resistor in an ordinary potentiometric circuit. The standard resistor was made of oxygen-free high-conductivity copper and had a resistance of 9.25×10^{-8} Ω. The feedback current through the standard resistor, or through the sample, was supplied by programmable constant-current sources (Hewlett-Packard No. 6177B) which were controlled either manually or by the output of the SLUG electronics. Typical currents were in the range 1–10 mA. All electrical connections to the tungsten samples were made by soldering to lead bands which had been electroplated onto the tungsten. We found that this procedure resulted in a tenacious low-resistance connection to the sample which could be cycled repeatedly to room temperature without degradation.[26] The contact resistance to the sample was found to be 10^{-7} to 10^{-9} Ω depending on the area of the lead band and the surface condition of the tungsten. The superconducting leads to the sample were made by tinning a twisted pair of No. 36 Manganin wires with lead-tin solder; the thermal conductivity of these wires was negligible in comparison to that of the tungsten so that the presence of the leads did not distort the temperature profile along the specimens.

During each run, data was taken in the following sequence. First, the temperature of the copper block was stabilized at a temperature T_0 and the values of R_1 and $\Delta R = R_1 - R_2$ were calibrated against the germanium standard thermometer at this temperature. Next the electrical resistance of the sample was measured. Then the sample heater was turned on and the temperature regulator was trimmed (if necessary) to make sure that the value of R_1 was equal to its original value. The new value of ΔR was then recorded and the thermo-

TABLE I. Summary of electrical and physical properties of all tungsten specimens.

Sample	RRR[a]	ρ_0 (10^{-11} Ω cm)	K_{max} (W/cm K)	A^b ($K^{1/2}$ V^{-1})	B^b (K^{-1} V^{-1})	Diameter (mm)	Length[c] (cm)
W-7	77 300	6.958	687	−0.13	0.386	2.84	7.62
W-6	62 700	8.587	638	0.06	0.232	3.00	5.08
W-3	44 200	12.18	494	1.22	0.2175	1.50	7.62
W-ϕ	29 200	18.42	•••	0.68	0.170	7.11	4.45
W-5	9 001	59.77	147	6.42	0.1213	1.50[d]	5.08

[a] $\rho(300\ \mathrm{K}) = 5.38\ \mu\Omega$ cm.
[b] $G(T) = AT^{-1/2} + BT^{+1}$, $T < 4$ K.
[c] Distance between probes on sample.
[d] Square cross section.

electric voltage across the sample was measured. Finally, $G(T)$ was obtained by balancing the galvanometer current to zero as previously described.

IV. EXPERIMENTAL RESULTS

The thermoelectric and transport properties of five high-purity tungsten specimens were measured over the temperature range 1.2–7 K. All of the specimens, except one,[27] were thin cylindrical rods with diameters ranging between 1.5 and 7.0 mm. The samples were single crystals, prepared by electron-beam zone refining,[28] with the [110] crystalline axis oriented parallel to the rod axis. The residual-resistivity ratio (RRR) $\rho(290)/\rho(0)$ of the samples varied between 9000 and 77 000; the electrical and physical properties of the samples are summarized in Table I. Data in the experiment were obtained at 0.1-K intervals according to the procedure described in Sec. III. At each temperature, measurements were made of the following quantities: the electrical resistivity $\rho(T)$, the thermal resistivity $W(T)$, the thermoelectric power $S(T)$, and the thermoelectric function $G(T)$ discussed in Sec. II.

Measurements of the electrical and thermal resistivity of four of these specimens have been reported in earlier work by Wagner, Garland, and Bowers (WGB).[6] In this experiment (approximately two years after WGB) these measurements were repeated and it was found that the residual resistivity of the highest-purity sample, W-7, had increased by 23%, while no significant change was noted for the other samples. A deterioration with age of the electrical purity of tungsten has been reported by Walsh,[29] who noticed that the amplitude of Azbel-Kaner cyclotron-resonance signals in tungsten showed a marked decrease over several months in high-resistivity-ratio samples. This effect was attributed[30] to the formation of a mosaic crystal structure in very pure material (resulting from the zone-refining process) which led to an enhanced amount of small-angle scattering at low temperatures. This explanation is consistent with our observation of a similar, though smaller, effect on the residual resistivity, a quantity which is relatively insensitive to small-angle scattering.

In Fig. 4, the temperature-dependent component of the electrical resistivity $\Delta\rho(T) = \rho(T) - \rho(0)$ is shown for samples W-3, W-5, and W-6, and it should be noted that Matthiessen's rule is well obeyed to within the resolution of the data.[31] As noted by WGB,[6] the electrical resistivity of tungsten at low temperatures can be satisfactorily described by a polynomial of the form

$$\rho(T) = \rho(0) + aT^2 + bT^5 , \tag{55}$$

where the quadratic term is dominant in this temperature range, as shown by the dashed line in Fig. 4.

We have found WT, the product of the thermal

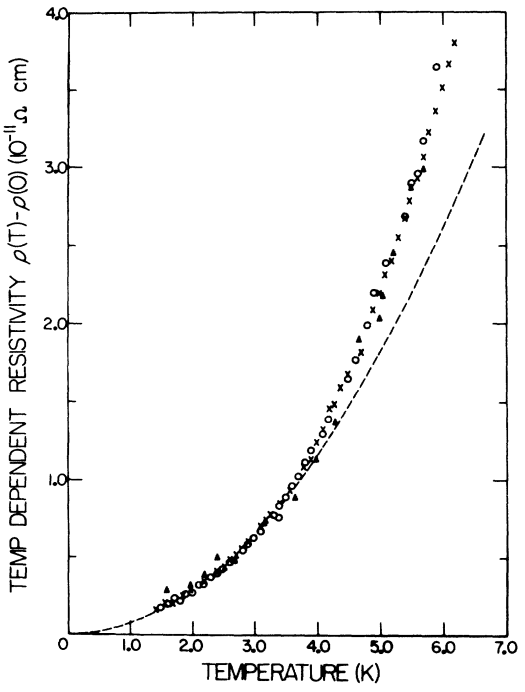

FIG. 4. Temperature-dependent component of the electrical resisitivity of tungsten samples W-3 (open circles), W-5 (closed triangles), and W-6 (crosses), showing conformity to Matthiessen's rule. The dashed line represents the quadratic function $(7.25\times10^{-13}\ \Omega\ \mathrm{cm/K^2})T^2$.

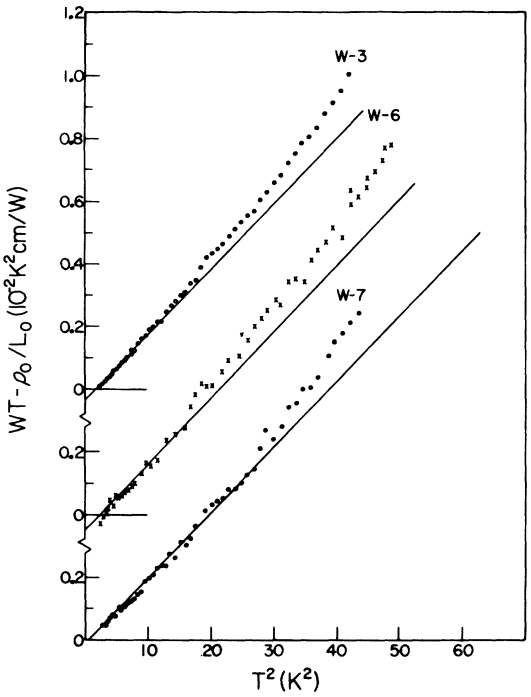

FIG. 5. Temperature-dependent thermal resistivity $(WT-\rho_0/L_0)$ of tungsten samples W-3, W-6, and W-7. The data for each sample have been displaced vertically for clarity.

resistivity and temperature, of all of our samples to have a predominantly quadratic temperature dependence. However, in contrast to Refs. 6 and 14 we have also observed the onset of a stronger power-law dependence in this temperature range. This is shown in Fig. 5, where the temperature-dependent part of the thermal resistivity $WT-(WT)_0$ is plotted as a function of T^2 for samples W-3, W-6, and W-7. The thermal resistivity of all of our specimens can be satisfactorily described by the expression

$$WT=(WT)_0+\alpha T^2+\beta T^3\,, \tag{56}$$

where the coefficients α and β were found to have the same value for each specimen within experimental error. The cubic term in Eq. (56) was chosen by analogy to the bT^5 term in Eq. (55); clearly the resolution of the data is not sufficient to distinguish a T^3 term from some other power-law dependence, for example T^4. For each sample, the extrapolated value of $(WT)_0$ agrees to within a few percent to the quantity ρ_0/L_0 expected from the zero-temperature limit of the Wiedemann-Franz law; this is in accord with the results of Ref. 6.

The temperature dependence of the thermoelectric function $G(T)$ defined by Eq. (3) is shown in Fig. 6 for all of the samples, and it is clear that this quantity is strongly dependent upon the electrical quality of the specimen. We will first consider the variation of $G(T)$ in the temperature range below about 4 K. In the highest-resistivity-ratio samples, W-6 and W-7, $G(T)$ increased nearly linearly with temperature up to about 3.5 K. In the lower-resistivity-ratio specimens, W-3, W-0, and W-5, a qualitatively different inverse temperature dependence began to appear which was most pronounced in the lowest-purity specimens. We have found that in this temperature range $G(T)$ can be adequately described for all samples by a two term polynominal of the form

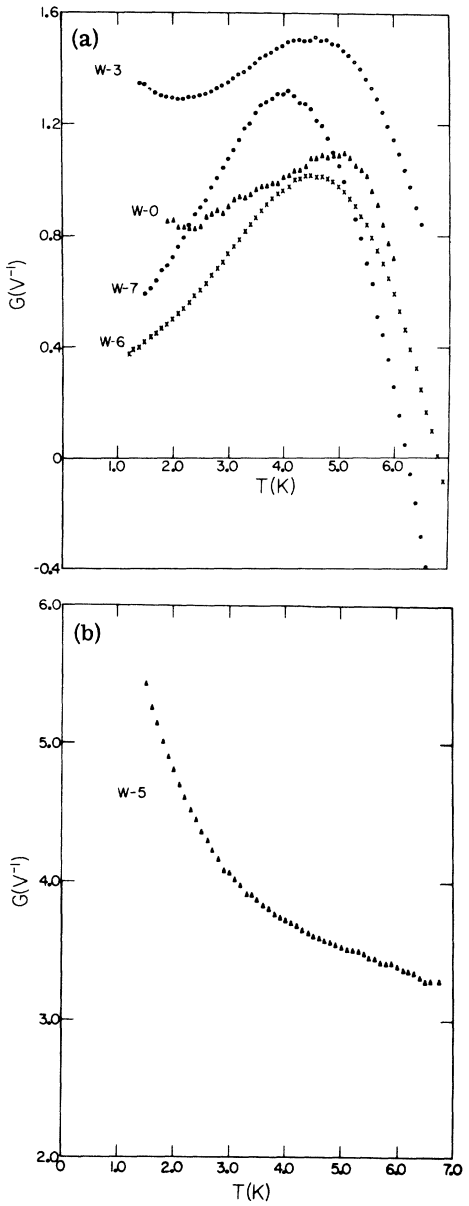

FIG. 6. (a) Thermoelectric function $G(T)$ for tungsten samples W-3, W-6, W-7, and W-0. (b) Thermoelectric function $G(T)$ for tungsten sample W-5.

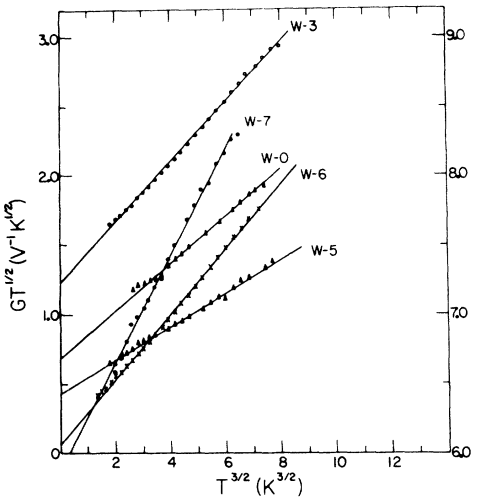

FIG. 7. Thermoelectric function $G(T)$ in the low-temperature region $T<4$ K for all specimens, plotted to illustrate the fit of the data to Eq. (57). The data for sample W-5 are associated with the right-hand ordinate.

$$G(T)=AT^{-1/2}+BT \quad (T<4\ \text{K}), \tag{57}$$

where A and B are coefficients which vary from sample to sample.[32] This is shown in Fig. 7, where the quantity $GT^{1/2}$ is plotted as a function of $T^{3/2}$ for all samples: The intercepts give the coefficient A while B is obtained from the slope of the lines. The values of these coefficients are listed in Table I, while their dependence on residual resistivity is shown in Fig. 8(a); it is clear that there is a general tendency for A to increase and for B to decrease with increasing impurity content. While this result appears to suggest a competition between multiple scattering processes in the metal, we note that there is an evident failure of the Nordheim-Gorter rule [Eq. (43)] at the higher-impurity levels. This is shown in Fig. 8(b), where $G(2K)$ is plotted against ρ^{-1} for all of the samples.

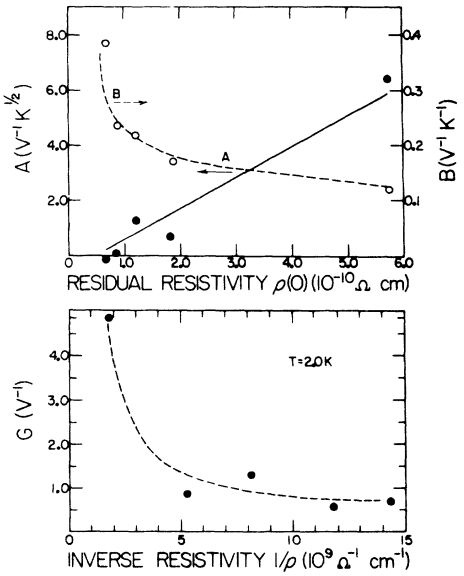

FIG. 8. (a) Dependence on residual resistivity of the coefficients A and B, defined by Eq. (57), for all specimens. (b) Dependence of $G(2K)$ on inverse resistivity for all specimens illustrating the failure of the Nordheim-Gorter rule.

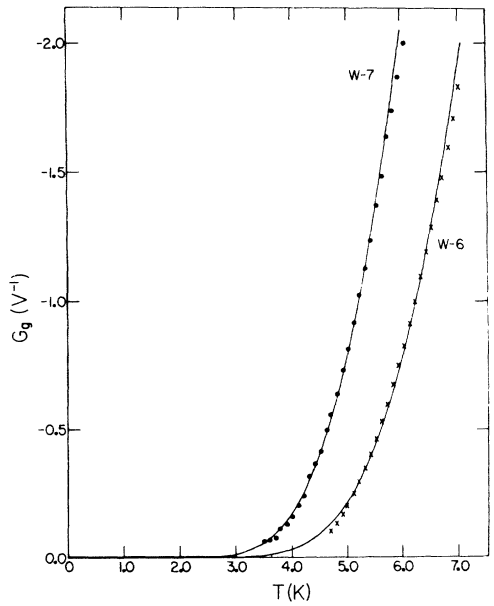

FIG. 9. Phonon-drag contribution to $G(T)$ for tungsten samples W-6 and W-7; the data points were obtained according to the procedure described in the text. The solid lines represent the best fit of Eq. (58) to the data using, for W-6, $K=0.008$ $V^{-1}K^{-2}$ and $\Theta_0=47$ K and, for W-7, $K=0.010$ $V^{-1}K^{-2}$ and $\Theta_0=38$ K.

Above 4 K there is the onset of a different temperature dependence for $G(T)$ which we observed for all specimens and which leads to a sign reversal in $G(T)$ at higher temperatures. We have found that all of our data above 4 K may be adequately described by an expression of the form

$$G_g(T)=-KT^2F(T/\Theta_0), \tag{58}$$

where $G_g(T)$ is obtained by subtracting from $G(T)$ the low-temperature terms $AT^{-1/2}+BT$, and $F(T/\Theta_0)$, defined by Eq. (67), is a function which is characteristic of the onset of electron-phonon interband processes. The temperature dependence of $G_g(T)$ of samples W-6 and W-7 is shown in Fig. 9; the solid curves correspond to the temperature dependence of Eq. (58) with K and Θ_0 treated as adjustable parameters. The data for the remaining samples exhibited, to within experimental uncertainties, the same temperature dependence as the data for W-6. As discussed in Sec. V we

identify this high-temperature effect as the onset of a phonon-drag mechanism.

Figure 10 shows the temperature dependence of the absolute thermoelectric power for samples W-3, W-5, W-6, and W-7; thermopower data for W-0 could not be obtained because of the large diameter of this specimen. As discussed in Sec. II, the ratio between S and G is a measure of inelastic scattering, i.e.,

$$\frac{S/L_0T}{G} = \frac{L}{L_0} . \tag{59}$$

In Fig. 11, the temperature dependence of L/L_0 obtained in this way is shown for samples W-3, W-5, W-6, and W-7. As expected for inelastic electron-phonon scattering, the ratio L/L_0 tends toward the classical elastic limit at zero temperature. The scatter in the data of Fig. 11 is almost entirely due to thermometry errors resulting from the measurement of the thermoelectric power.[33]

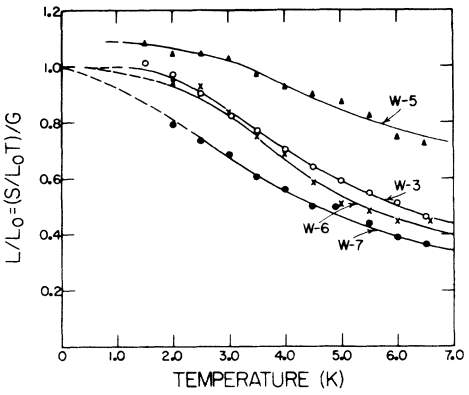

FIG. 11. Temperature dependence of the Wiedemann-Franz ratio for tungsten samples W-3, W-5, W-6, and W-7.

V. DISCUSSION

We have found that below about 4 K the temperature dependence of the electrical resistivity ρ and the thermal resistivity WT of tungsten increases nearly as T^2. Above 4 K there is a deviation from the quadratic power-law dependence of the data which can be adequately described by an additional T^5 term for ρ and a T^3 term for WT. The most straightforward explanation of these results is to attribute the low-temperature quadratic behavior of ρ and WT to electron-electron scattering, and to explain the additional higher-temperature terms on the basis of a Bloch-Grüneisen model for electron-phonon scattering. It is generally believed, however, that the resistivity resulting from electron-phonon scattering in a polyvalent transition metal with a multisheet Fermi surface has a more complicated temperature dependence than the simple power-law expression of the Bloch-Grüneisen theory. Thus, for tungsten, we do not believe it is possible to make an unambiguous association of a particular power-law component of ρ or WT with a specific scattering mechanism solely on the basis of resistivity measurements. As will be shown, we have found no corroborating evidence from measurements of the thermoelectric properties of tungsten that electron-electron scattering is significant in this temperature range; instead, it seems more likely to us that the low-temperature quadratic temperature dependence of ρ and WT is a consequence of the electron-phonon interaction.

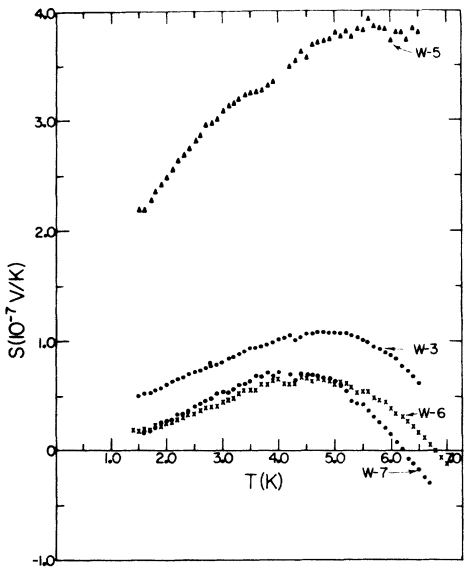

FIG. 10. Temperature dependence of the thermoelectric power $S(T)$ for tungsten samples W-3, W-5, W-6, and W-7.

From our measurements of the electrical and thermal resistivity we have found no measurable deviations from Matthiessen's rule (DMR) for almost a tenfold variation in the residual resistivity of our samples. We believe this to be a rather surprising result in view of the striking DMR observed in most high-purity metals in this temperature range.[34] Recent studies of DMR in dilute alloys of aluminum,[35,36] indium,[37] and gallium[38] have shown that in each case the DMR, $\Delta\rho$, can be expressed as a cubic function of temperature with a logarithmic dependence on residual resistivity, i.e.,

$$\Delta\rho \cong AT^3 \ln\rho_0 , \tag{60}$$

and it has been suggested recently that this expression may be applicable to all polyvalent metals with Fermi surfaces of two or more sheets.[38] Our results indicate that this conjecture is not correct, at least insofar as tungsten is concerned, and that

the suggestion, by Bass,[34] that Eq. (60) may be an accidental result of curve-fitting procedures deserves further consideration.

Our measurements of the thermoelectric properties of tungsten show a pronounced peak in both $S(T)$ and $G(T)$ at about 4 K followed by a sign reversal at higher temperatures. In the subsequent discussion, we will consider primarily the temperature dependence of $G(T)$ rather than $S(T)$ because of the higher resolution of the $G(T)$ data. Colquitt, Fankhauser, and Blatt[13] (CFB) have remarked that a low-temperature peak in the thermoelectric power of a transition metal can in some circumstances result from interband electron-electron scattering. Although the "intrinsic" thermopower arising from electron-electron scattering alone has a linear temperature dependence, with multiple scattering the observed electron-electron contribution to the total thermopower will be weighted according to the Nordheim-Gorter rule i.e.,

$$S_{ee} = S_{ee}^{i} W_{ee}/W_{\text{tot}} , \tag{61}$$

where S_{ee}^{i} is the intrinsic thermopower due to e-e processes, and W_{ee} is the corresponding component of the thermal resistivity. Both S_{ee}^{i} and W_{ee} have a linear temperature dependence and, if impurity scattering is neglected, $W_{\text{tot}} = aT + bT^{n}$, where n characterizes the contribution to the thermal resistivity from electron-phonon scattering. CFB have shown that Eq. (61) predicts a low-temperature peak in S_{ee}; whether or not this could actually be observed depends on the magnitudes of both the impurity contribution and the electron-phonon contribution to the total thermopower. We do not believe that this explanation can be used to account for the peak in $S(T)$ and $G(T)$ observed in tungsten.

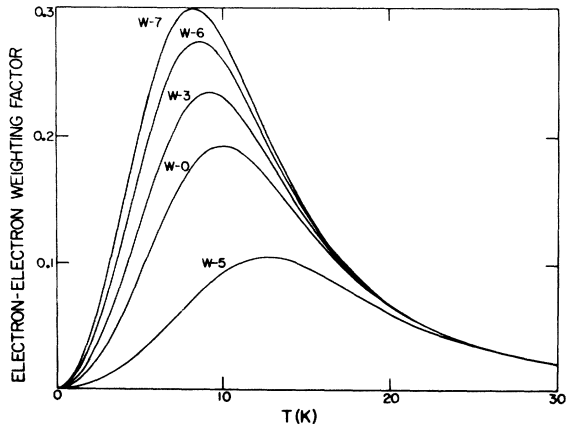

FIG. 12. Temperature dependence of the electron-electron weighting factor, defined by Eq. (62), for all samples.

The expression for G_{ee} which corresponds to Eq. (61) is, according to Eq. (42),

$$G_{ee} = G_{ee}^{i} \rho_{ee}/\rho_{\text{tot}} , \tag{62}$$

where the intrinsic electron-electron component G_{ee}^{i} is independent of temperature, ρ_{ee} is proportional to T^2, and the total resistivity can be written as in Eq. (55).[39] In contrast to Eq. (61), this expression does not allow for a peak in G_{ee} in the high-purity limit $\rho_0 = 0$; however, for moderate impurity levels, a peak in G_{ee} can occur at low temperatures. This is shown in Fig. 12, where the electron-electron weighting factor $aT^2/(\rho_0 + aT^2 + bT^5)$ is plotted as a function of temperature for each of our specimens. It should be noted that in the temperature range below 4 K, G_{ee} has a temperature dependence which is predominantly quadratic. We find no evidence of such a quadratic term in $G(T)$ for any of our samples; instead, as noted in Sec. IV, $G(T)$ in the temperature range from 1 to 4 K appears to increase nearly linearly with temperature in the highest-purity specimens, and as $T^{-1/2}$ in the lower-purity specimens. In this regard, we also note that these two temperature components do not scale with sample resistivity according to the Nordheim-Gorter rule. As a result, we do not believe it is possible to identify either the T^1 or the $T^{-1/2}$ term with a particular scattering mechanism. A more plausible explanation is to attribute these two terms to contributions to $G(T)$ from different sheets of the Fermi surface. In this case, each component of $G(T)$ would incorporate the effects of all scattering mechanisms rather than a single scattering component. An expression for $G(T)$ for multiple scattering in a multiband conductor may be easily derived by combining Eq. (42) and Eq. (45). The result, however, is not easily evaluated since it involves detailed knowledge of the transport coefficients of each band which result from every scattering mechanism. In the high-purity limit, however, the expression for $G(T)$ reduces simply to Eq. (45). For electron-electron scattering in a multiband conductor this is

$$G(T) = W_{\text{tot}} \sum_{i} \frac{G_{ee}^{i}}{W_{ee}^{i}} , \tag{63}$$

where G_{ee}^{i} is the intrinsic contribution on band i to $G(T)$ from electron-electron scattering, and W_{ee}^{i} is the corresponding thermal resistivity. From Eq. (63) $G(T)$ is temperature independent to lowest order if the impurity term in W_{tot} is neglected, and has a T^{-2} dependence if it is included. We therefore find no reasonable way to account for the linear temperature dependence of $G(T)$ observed in high-purity specimens on the basis of electron-electron scattering. Instead, we believe the electron-phonon interaction is a more likely cause of

the observed results in high-purity specimens. Unfortunately, we cannot determine the temperature dependence for $G(T)$ characteristic of electron-phonon scattering without including specific details of the tungsten Fermi surface, and allowing for the important effect of umklapp processes on both G_{ep} and W_{ep}.[39] Because the data for pure specimens has such a simple linear temperature dependence, however, it seems likely that there is a single dominant contributor to $G(T)$ in this temperature range; if this is correct, then additional theoretical work on this problem would appear to have attractive possibilities.

The $T^{-1/2}$ dependence of $G(T)$ observed in the lowest-purity samples below 4 K cannot be explained by any simple model of impurity scattering; as discussed in Sec. II, the contribution to $G(T)$ from impurity scattering is independent of temperature. We believe that the $T^{-1/2}$ term in $G(T)$ is probably also a consequence of electron-phonon scattering, and that the electrical purity of all the samples is too great to permit the impurity contribution to $G(T)$ to become predominant. In this regard we remark that while the resistivity of all of our samples in this temperature range was dominated by impurity scattering,[40] even the lowest-purity specimen, W-5, had a residual resistance ratio of 9000 and an estimated impurity content of only several parts per million. We are unable to account for the enhancement of the $T^{-1/2}$ term with increasing impurity content, however, a result which is in conflict with the Nordheim-Gorter rule. If the T^1 and the $T^{-1/2}$ terms are interpreted as electron-phonon contributions to $G(T)$ from different sheets of the tungsten Fermi surface, then the observed impurity dependence of these terms could be explained only by supposing that the addition of impurities of the metal acted preferentially on the transport processes of one of the sheets. While this seems unlikely for isotropic impurity scattering, it is possible that boundary scattering could lead to such a result in size-limited specimens.

At temperatures above 4 K, $S(T)$ and $G(T)$ for all samples was found to exhibit a qualitatively different temperature dependence, eventually becoming negative in the highest-purity specimens. We attribute this high-temperature behavior to the onset of a phonon-drag mechanism whose peak is reported to occur at about 70 K.[11] The onset of phonon drag is usually observed to contribute a T^3 component to the thermoelectric power or, from Eq. (4), a T^2 component to $G(T)$. While our data for $G(T)$ tend toward a quadratic temperature dependence at the highest temperatures, the onset of the effect occurs with a much stronger power-law dependence. We believe this result can be explained on the basis of interband scattering between hole and electron sheets of the tungsten Fermi surface. rf size-effect measurements[41] indicate that a gap, resulting from spin-orbit coupling,[42] exists between the balls of the electron jack, centered at Γ in the Brillouin zone, and the hole octahedra located along the six equivalent $\langle 100 \rangle$ directions. This gap suggests that phonon-induced interband transitions can occur only for phonon energies greater than a minimum threshold energy, and we believe this can lead to the sudden onset observed in the phonon-drag contribution to $G(T)$. The allowed interband transitions are given in Fig. 13, which shows a stylized projection of the Fermi surface of tungsten on the (001) plane. We are assuming a nonequilibrium phonon distribution corresponding to a heat current $\vec{J}_Q$ along the [110] direction, and we want to determine what electric current will result when these excess phonons are absorbed by the electron system. As shown in Fig. 13, there are two energetically favorable interband processes which can occur at low temperatures, corresponding, respectively, to the creation and annihilation of electron-hole pairs; in each process, a phonon is absorbed which has a wave-vector component along the [110] direction. The inverse (phonon emission) processes are also possible of course, but occur with equal probability only in the absence of a temperature gradient, as required by detailed balance considerations. In the pair-creation process, an excited electron $\vec{k}_e$ is created at the $[\bar{1}00]$ gap while a hole excitation $\vec{k}_h$ is created at the [100] gap. In order to conserve crystal momentum a phonon with wavevector $\vec{q}$ must be absorbed such that $\vec{q} = \vec{k}_e + \vec{k}_h$, and it can be seen from the figure that $\vec{q}$ must be sufficiently large to span the gap between the hole and electron surfaces. An identical creation

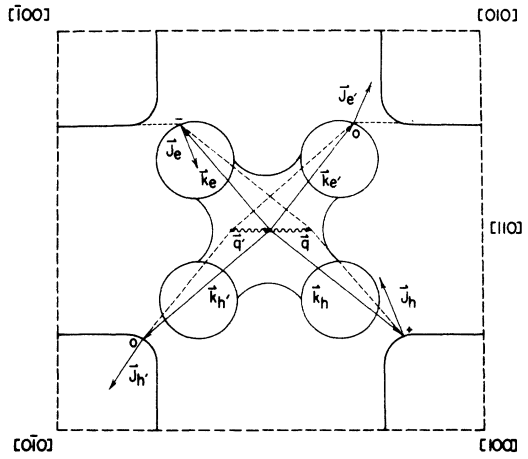

FIG. 13. Schematic projection of the Fermi surface of tungsten on the (001) plane showing the allowed interband transitions which result in the absorption of [110] phonons.

process (not shown in the figure) will occur at the $[0\bar{1}0]$ and $[010]$ gaps, and from symmetry the contribution to the total current from these two processes must lie along the $[110]$ direction. Whether this current is positive or negative depends on the relative magnitude of the Fermi velocities on the electron and hole surfaces near the gap; for $v_F^h > v_F^e$, the resultant current will be negative and this will lead to a negative phonon-drag contribution to $G(T)$.

In the other phonon absorption process, an electron in a filled state with wave vector $\vec{k}_e'$ is destroyed at the $[010]$ gap while a simultaneous hole vacancy $\vec{k}_h'$ is created at the $[0\bar{1}0]$ gap. For this case, momentum conservation requires that $\vec{q}' + \vec{k}_e' + \vec{k}_h' = 0$, while the direction of the resultant current again depends on the relative Fermi velocities on the hole and electron surfaces. Energy is conserved in the transition inasmuch as the absorbed phonon is required to make up the deficit between the energy gained in removing an electron from $\vec{k}_e'$ and the energy expended in establishing a hole vacancy at $\vec{k}_h'$. Identical transitions (not shown in the figure) occur at the $[100]$ and $[\bar{1}00]$ gaps and cancel all but the $[110]$ component of current. On the $\langle 100\rangle$ axes, the Fermi velocity on the hole octahedron is found from energy-band calculations[43] to be slightly greater than that on the adjacent electron jack. Since the Fermi surface is roughly spherical in the vicinity of these points, the total current is dominated by the hole carriers. Hence, $\vec{J}$ and $\vec{J}_Q$ will be oppositely directed and the electron-hole interband transitions will give rise to a negative phonon-drag contribution to $G(T)$ and $S(T)$. It can be shown that at higher temperatures at which long-phonon-wave-vector absorptions occur, both the hole and electron sheets contribute negatively to $G(T)$ and the relative Fermi velocities are not critical.

A simple model of electron-hole transitions gives a good qualitative fit to the data above 4 K. The phonon-drag contribution to the thermopower S_g is proportional to the lattice specific heat C_v, which for a Debye solid can be written as[4]

$$C_v = 3Nk \int_0^{\omega_D} \frac{(\hbar\omega/kT)\, e^{\hbar\omega/kT}}{(e^{\hbar\omega/kT}-1)^2}\, C(\omega)\, d\omega \,, \qquad (64)$$

where $C(\omega)$ is the fractional phonon density of states given by $C(\omega) = 3\omega^2/\omega_D^3$ and ω_D is the Debye frequency. Setting $S_g = C_v/3Ne$ and making use of Eq. (64) and Eq. (4), we obtain

$$G_g(T) = \frac{3k}{eL\Theta_D}\left(\frac{T}{\Theta_D}\right)^2 \int_0^{\Theta_D/T} dx\, \frac{x^4 e^x}{(e^x-1)^2} \,, \qquad (65)$$

where the Debye temperature $\Theta_D = \hbar\omega_D/k$. At temperatures $T \ll \Theta_D$, $G_g(T)$ has the anticipated quadratic temperature dependence. We account for the phonon wave vector threshold for interband transitions by assuming that only phonons of frequency $\omega > \omega_0$ can transfer momentum to the electrons.

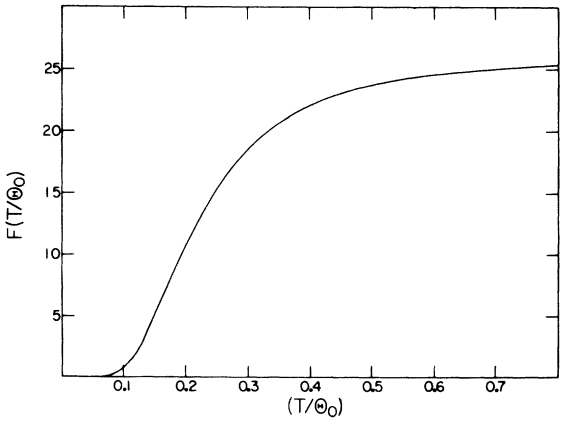

FIG. 14. Temperature dependence of the weighting factor $F(T/\Theta_0)$ defined by Eq. (67).

Thus the lower limit of the integral in Eq. (65) can be replaced by Θ_0/T, where $\Theta_0 = \hbar\omega_0/k$. It is convenient to change variables to $y = 1/x$ so that Eq. (65) becomes, for $T \ll \Theta_D$ and $\Theta_0 \ll \Theta_D$,

$$G_g(T) = \frac{3k}{eL\Theta_D}\left(\frac{T}{\Theta_D}\right)^2 F\left(\frac{T}{\Theta_0}\right), \qquad (66)$$

where

$$F(T/\Theta_0) = \int_0^{T/\Theta_0} dy\, \frac{1}{y^6}\, \frac{e^{1/y}}{(e^{1/y}-1)^2} \,. \qquad (67)$$

The temperature dependence of the weighting factor $F(T/\Theta_0)$ is shown in Fig. 14, and it should be noted that the onset of interband transitions begins at temperatures well below the threshold temperature Θ_0. For our samples, phonon drag began to appear at about 4 K, corresponding to a cutoff of $\Theta_0 \approx 45$ K. Recent calculations of the phonon dispersion relations in tungsten[44] suggest the existence of a transverse-acoustic-phonon mode along $\langle 110\rangle$ corresponding to $\Theta_0 = 45$ K at wave vector $q \approx 0.1$ Å^{-1}, which should be the gap between the electron and hole sheets in the $\langle 100\rangle$ directions. This agrees with rf size-effect measurements[41] which set the gap at approximately 5% of the total distance from the center of the zone to the zone vertex along the $[100]$ direction (1.987 Å^{-1}). While this phonon-drag model reproduces satisfactorily the qualitative features of our data, agreement in detail would require considering the true phonon spectrum for tungsten and the $\vec{k}$ dependence of the Fermi velocities on the hole octahedra and electron-jack balls. We have also implicitly assumed that the phonon gas transfers essentially all of its momentum to the conduction electrons, which ignores phonon-phonon scattering. This assumption is probably reasonable in the temperature range investigated in this experiment.

ACKNOWLEDGMENTS

The authors have profited from several helpful discussions with Dr. D. K. Wagner, Dr. M. Yaqub, Dr. C. A. Ebner, and in the earliest phase of the work, with Professor A. B. Pippard. We are also grateful for the expert technical assistance of R. L. Kindler.

APPENDIX

The equilibrium or steady-state analysis of the experiment for measuring $G(T)$—shown schematically in Fig. 1—has been outlined in Sec. III. We now wish to consider the response of the experiment to transient deviations from equilibrium. As in any direct-coupled system which employs negative feedback, there is a mandatory compromise between the dc gain and the frequency response of the system. While it is desirable for the gain to be as great as possible in order to minimize inherent feedback error [cf Eq. (51)], the gain cannot be increased indefinitely without eventually precipitating some kind of dynamic instability; this instability results from the phase shifts which are an inevitable consequence of the high-frequency "roll-off" characteristics of the system. In this experiment, the high-frequency response is essentially limited by the resistance R of the sample and the inductance L_0 of the superconducting loop shunting the sample. A typical value of L_0 was about 10^{-8} H while R varied between 10^{-8} Ω and 10^{-9} Ω, corresponding to an "intrinsic" time constant $\tau_1 = L_0/R$ of 1–10 sec. The contact resistance r between the superconducting loop and the sample tends to reduce the observed time constant from this intrinsic value somewhat, although loop time constants as great as 5 sec were noted for some of the larger-diameter samples. In addition to the intrinsic time constant τ_1, the response of the instrumentation may be tailored to enhance stability and to attenuate noise; in this experiment the instrumentation time constant τ_0 was determined by a single-section RC filter and could be adjusted between 0.01 and 1 sec. Figure 15 shows an equivalent-circuit representation of the experiment, in which the sample is considered to be a resistance R in series with a voltage source $\Delta V(\omega)$, L_0 is the inductance of the superconducting loop which shunts the sample, r is the total contact resistance between the loop and the sample, and the instrumentation is represented as a current amplifier with gain β. As already mentioned there are two characteristic time constants, $\tau_0 = R_0 C_0$ and $\tau_1 = L_0/R$; the real time constant of the sample-superconductor loop is $L_0/(R+r)$, but this quantity is of no practical importance since it does not characterize the response of the loop when it is operating in a feedback mode.

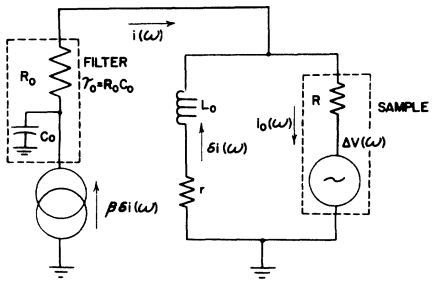

FIG. 15. Equivalent-circuit representation used for analyzing the dynamic response of the experiment.

According to Kirchoff's law, the voltages around the sample-superconductor loop must sum to zero, resulting in

$$-\Delta V(\omega) + i_0(\omega) R + \delta i(\omega)(r + j\omega L_0) = 0 , \qquad \text{(A1)}$$

where current conservation requires $i(\omega) + \delta i(\omega) = i_0(\omega)$. The "filtered" current from the amplifier $i(\omega)$ is related to the "unfiltered" current $\beta\delta i(\omega)$ according to Ohm's law, i.e.,

$$i(\omega) = \gamma\beta\delta i(1 - j\omega\tau_0) , \qquad \text{(A2)}$$

where $\gamma \equiv (1 + \omega^2\tau_0^2)^{-1}$. Solving Eqs. (A1) and (A2) for $i(\omega)$ results in

$$i(\omega) = \frac{\gamma\beta(1 - j\omega\tau_0)\Delta V(\omega)/R}{(\gamma\beta + r/R + 1) + j\omega(\tau_1 - \gamma\beta\tau_0)} . \qquad \text{(A3)}$$

In the low-frequency limit, Eq. (A3) reduces to Eq. (50), i.e.,

$$i(0) = \frac{\beta}{\beta + 1 + r/R}\,(\Delta V/R) ,$$

while at nonzero frequencies $i(\omega)$ is both attenuated and shifted in phase with respect to the "excitation" voltage $\Delta V(\omega)$. Because the time constant τ_1 is typically several seconds, this attenuation is very pronounced, even at low frequencies, so that dynamic measurements of G cannot be made without incurring an excessive measurement error.

Of more importance, however, is the effect of the phase shifts introduced by τ_0 and τ_1 on the stability of dc measurements of G. We adopt the following criteria for stability[45]: (i) The experiment will be regenerative, although not necessarily unstable, at all frequencies corresponding to $|1 - M| < 1$, where M is the complex loop gain, [46] and (ii) the experiment will be unstable (i.e., oscillate) at any frequency for which M becomes both real and greater than unity.

In this experiment M is given by

$$M = \left(\frac{-1}{1 + r/R + j\omega\tau_1}\right)\left(\frac{\beta}{1 + j\omega\tau_0}\right) , \qquad \text{(A4)}$$

with a frequency-dependent phase angle given by

$$\tan\phi = \frac{\omega\tau_0(1+r/R+\tau_1/\tau_0)}{1+r/R-\omega^2\tau_0\tau_1} \quad . \tag{A5}$$

Inspection of Eq. (A5) reveals that the phase shift can never reach 180°, so that oscillations will not occur for any values of τ_0, τ_1, or r/R. However, M will always enter the regenerative region characterized by criterion (i) at sufficiently high frequencies; whether transient instabilities (ringing) or other troublesome effects will actually occur depend on how close M approaches the critical point, $M=+1$. We have not found this to be a problem provided that the current gain β was kept below about 10^5 and that reasonable care was taken to ensure that the frequency response of the instrumentation was dominated by a single time constant τ_0 and not by stray reactive elements.

---

*Research supported in part by the National Science Foundation, Grant No. GH33385A1.

†National Science Foundation Graduate Fellow.

[1]References on the Fermi surface of tungsten may be found in R. F. Girvan, A. V. Gold, and R. A. Phillips, J. Phys. Chem. Solids 29, 1485 (1968); and W. M. Walsh, Jr., in *Solid State Physics*, edited by J. F. Cochran and R. R. Haering (Gordon and Breach, New York, 1968), Vol. I, pp. 145–188.

[2]N. F. Mott, Proc. R. Soc. A 156, 368 (1936).

[3]Reference 6 contains an extensive bibliography on the electrical and thermal resistivity of tungsten and other transition elements.

[4]J. M. Ziman, *Electrons and Phonons* (Oxford U. P., London, 1960).

[5]E. Bucher, F. Heiniger, and J. Muller, *Proceedings of the Nineth International Conference on Low Temperature Physics* (Plenum, New York, 1965), p. 1059.

[6]D. K. Wagner, J. C. Garland, and R. Bowers, Phys. Rev. B 3, 3141 (1971).

[7]D. K. Wagner, Phys. Rev. B 5, 336 (1972).

[8]A preliminary account of this work was given by J. C. Garland, Appl. Phys. Lett. 22, 203 (1973).

[9]V. Raag and H. V. Kowger, J. Appl. Phys. 36, 2045 (1965).

[10]J. J. Lander, Phys. Rev. 74, 479 (1948).

[11]R. Carter, A. Davidson, and P. A. Schroeder, J. Phys. Chem. Solids 31, 2374 (1970).

[12]D. M. Sparlin and J. A. Marcus, Phys. Rev. 144, 484 (1966).

[13]L. Colquitt, H. R. Fankhauser, and F. J. Blatt, Phys. Rev. B 4, 292 (1971).

[14]H. J. Trodahl (unpublished).

[15]J. Clarke, Phys. Today 24, No. 8, 30 (1971).

[16]Reference 4, p. 270.

[17]Although tensors in noncubic metals, for simplicity the transport coefficients will be treated as scalars in this discussion.

[18]R. D. Barnard, *Thermoelectricity in Metals and Alloys* (Wiley, New York, 1972), p. 62.

[19]J. M. Ziman, *Principles of the Theory of Solids* (Cambridge U. P., Cambridge, England, 1964).

[20]Reference 18, p. 76.

[21]Reference 18, p. 151.

[22]A. R. de Vroomen, C. van Baarle, and A. J. Cuelenaere, Physica (Utr.) 26, 19 (1960).

[23]Reference 18, p. 140.

[24]J. W. Ekin and D. K. Wagner, Rev. Sci. Instrum. 41, 1109 (1970).

[25]J. Clarke, Philos. Mag. 13, 115 (1965).

[26]D. J. VanHarlingen and J. C. Garland (unpublished).

[27]Sample W-5 was a rod with a square cross section.

[28]The specimens were supplied by B. Addis, Department of Metallurgical Engineering, Cornell University, Ithaca, N.Y.

[29]W. M. Walsh, Jr., *Solid State Physics*, edited by J. F. Cochran and R. R. Haering (Gordon and Breach, New York, 1968), Vol. I, pp. 127–252.

[30]W. M. Walsh, Jr. (private communication).

[31]The resistivity data for samples W-7 and W-0 are consistent with these results, but the scatter in the data is somewhat greater.

[32]Thermodynamic considerations require $G(T)T=0$ at zero temperature; thus $G(T)$ may diverge at low temperatures with a power-law dependence weaker than T^{-1}.

[33]Conventional measurements of L/L_0 are made by dividing $\rho(T)$ by WTL_0. Since the measurement of the thermal resistivity W involves the same thermometry difficulties as measurements of the thermoelectric power S, we expect the scatter of L/L_0 data to be about the same regardless of whether it is determined from ρ/WTL_0 or from S/GTL_0. We remark, however, that S and G can be independently obtained without knowledge of the cross-sectional area of the specimen.

[34]J. Bass, Adv. Phys. 21, 431 (1972).

[35]A. D. Kaplan and C. Rizzuto, J. Phys. C 3, L117 (1970).

[36]J. W. Ekin and B. W. Maxfield, Phys. Rev. B 2, 4802 (1970).

[37]I. A. Cambell, A. D. Kaplan, and C. Rizzuto, Phys. Rev. Lett. 26, 239 (1971).

[38]L. Morelli, R. I. Boughton, and J. E. Neighbor, J. Phys. F 3, L102 (1973).

[39]The characteristic temperature dependence of the transport coefficients which result from electron-electron scattering is believed to be nearly independent of Fermi-surface topography, depending instead primarily on the phase space available to the scattered electrons. [See, for instance, C. Hodges, H. Smith, and J. W. Wilkins, Phys. Rev. B 4, 302 (1971).] By contrast, the electron-phonon terms in the transport coefficients can be greatly affected by Fermi-surface anisotropy.

[40]We include scattering by lattice defects and sample boundaries in the category "impurity scattering." In the highest-resistance-ratio samples (W-6 and W-7), boundary scattering was probably as significant as impurity scattering in determining the residual resistivity.

[41]W. M. Walsh, Jr. and C. C. Grimes, Phys. Rev. Lett. 13, 523 (1964).

[42]L. F. Mattheiss and R. E. Watson, Phys. Rev. Lett. 13, 526 (1964).

[43]L. F. Mattheiss, Phys. Rev. A 139, 1893 (1965).

[44]A. O. E. Animalu, Phys. Rev. B 8, 3555 (1973).

[45]N. Nyquist, Bell System Tech. J. 11, 126 (1932).

[46]The loop gain $M(\omega)$ is defined as the signal that would be returned if the feedback loop were opened at any point and a unity signal were injected into the loop in the forward direction.